A Low Cost Navigation Unit for Positioning of Personnel After Loss of GPS Position

Kim Mathiassen*, L. Hanssen** and O. Hallingstad***
*University of Oslo/Department of Informatics, Oslo, Norway. Email: kimmat@ifi.uio.no
**Norwegian Defence Research Establishment, Kjeller, Norway. Email: leif.hanssen@ffi.no
***Norwegian University of Science and Technology/Department of Engineering Cybernetics, Trondheim, Norway. Email: oh@unik.no

***Abstract*—We have built a test unit containing a GPS, an inertial measurement unit, magnetometers and a barometer. When the GPS looses its signals, the other sensors are used to keep track of the position. Unscented Kalman filters have been used to test the performance of different aid sensor configurations. In addition to the four different sensor configurations, the gyroscope output was filtered, making it eight different test scenarios. Simulations show that filtering the gyroscope output and using inertial sensors in addition to a barometer had the lowest position error, with a standard deviation of the position of 8.5 m. For unfiltered gyroscope output the best result was obtained when using all sensors. This had a standard deviation of the position of approximatly 42 m. The preliminary real world test results had a much larger error than the simulation.**

I. Introduction

Low cost GPS devices have made it common to equip personnel, vehicles and other equipment with GPS to track their position. The GPS gives accurate position information when satellites are visible, but fails when it looses satellite signals. This might happen inside buildings, in urban areas and in highly vegetated areas. Micro-Electro-Mechanical Systems (MEMS) sensors are getting popular within consumer electronics [1], which leads to lower prices on MEMS sensors. By adding low cost inertial sensors, magnetometers and a barometer to the GPS-unit we want to track the position even when the satellites are not visible. This article focuses on the possible gain by adding magnetometers and a barometer in addition to the inertial sensors.

Many research projects have been conducted over the last years to find solutions to the problem mentioned above. [2] has created a personal navigation system using an inertial measurement unit (IMU), magnetometers, a barometer and a Doppler radar. The Doppler radar measures the velocity of the person relative to the environment. The system is intended to track ground soldiers in the U.S. Army during operations. They showed that the Doppler radar had significant impact on the position accuracy. [3], [4] uses an IMU, a magnetometer and a GPS to create a pedestrian navigation system. These articles states that the main error source in positioning is the determination of the azimuth and uses knowledge of walking characteristics to estimate the azimuth using a Kalman filter.

To limit the drift systems that estimate the step length and direction has been developed. [5] uses a IMU and magnetometer placed on the foot of a person, and uses two approaches. The first is Zero Velocity Updates. The second approach is to estimate the number of steps, stride length and heading to calculate the position. [6] has created a system for first responders that use similar sensors, but a different method for step and stride estimation. A system for positioning of dismounted soldiers is presented in [7]. This system uses an IMU, magnetometers and a barometer and is able to distinguish between steps going forwards, backwards and sideways.

In this article we will analyse a multipurpose navigation unit that can be used in areas with difficult satellite signal conditions. We have tested the performance of the test unit with the use of different sensor configurations, both in simulation and in the real world, in order to find out how different sensor configuration affect position accuracy and how long it is possible for the navigation system to have a good estimate of the position.

A. Outline

In Section II relevant theory will be reviewed. In Section III the developed test unit will be described. In Section IV the navigation models will be derived. Section V contains the results and Section VI contains the conclusion.

II. Background

This sections reviews the relevant theory used in this article.

A. Reference Frames

In order to model the navigation equations for a strapdown navigation system we define four different reference frames. First is the *Earth Centered Inertial* (ECI) frame, denoted with a superscript i. This frame fulfills the laws of Newton mechanics and is centered to earth and shares its polar axis[8].

The second frame is the *earth-centered-earth-fixed* frame (ECEF), and is denoted with a superscript e. We use the World Geodetic System 1984 (WGS-84) model as our earth model [9]. The GPS receiver outputs the position in ellipsoidal coordinates of latitude ϕ, longitude λ and height h above the mean sea level, and we need methods to convert between the two. The conversion from ellipsoidal coordinates to Cartesian coordinates is straight forward, and given in [9]. To convert from Cartesian coordinates to ellipsoidal coordinates is more difficult, and only the longitude can be computed explicitly. The latitude and height above mean sea level is estimated through an iterative algorithm found in [10]. The algorithm is set to have an accuracy of 10^{-8}.

978-1-4244-5864-6/10$26.00

The *local-level* frame is a tangent plane on the WGS-84 ellipsoid, and is denoted with a superscript l. The local-level is an East-North-Up (ENU) frame.

The *body* frame is a right-handed three-dimensional Cartesian frame related to an object. In this case the object is the test unit and it is used as origin. The basis vectors $\boldsymbol{x}^b$, $\boldsymbol{y}^b$ and $\boldsymbol{z}^b$ is defined to be the same as the axis used by the ADIS16405 sensor on the test unit. This frame is used to determine the relative attitude with respect to the local-level frame.

1) Transformation Between the Earth Frame and the Local-Level Frame: The earth frame and the local-level frame does not have the same origin. If the coordinate $\boldsymbol{p}_0^e$ is the origin of the local-level frame given in earth frame coordinates, then the transformation of the coordinate $\boldsymbol{p}^l$ to the coordinate $\boldsymbol{p}^e$ is given by

$$\boldsymbol{p}^e = \boldsymbol{p}_0^e + \boldsymbol{R}_l^e(\phi, \lambda)\boldsymbol{p}^l \tag{1}$$

where $\boldsymbol{R}_l^e(\phi, \lambda)$ is the coordinate transformation matrix from the earth frame to the local-level frame and is given by

$$\boldsymbol{R}_l^e(\phi, \lambda) = \begin{bmatrix} -\sin\phi\sin\lambda & \cos\lambda & -\cos\phi\sin\lambda \\ -\sin\phi\cos\lambda & -\sin\lambda & -\cos\phi\cos\lambda \\ \cos\phi & 0 & -\sin\phi \end{bmatrix} \tag{2}$$

For a vector the transformation is given by [9]

$$\boldsymbol{v}^e = \boldsymbol{R}_l^e(\phi, \lambda)\boldsymbol{v}^l \tag{3}$$

2) Transformation Between the Local-Level Frame and the Body Frame: For simplicity the origin of the local-level frame and the body frame is defined to be the same. The coordinate transformation matrix $\boldsymbol{R}_b^l$ transforms from the local-level frame to the body frame. We will use quaternions to represent the attitude and the coordinate transformation matrix will be calculated from [11]

$$\boldsymbol{R}(\boldsymbol{q}_b^l) = \boldsymbol{I} + 2\eta\boldsymbol{\epsilon}^\times + 2\boldsymbol{\epsilon}^\times\boldsymbol{\epsilon}^\times \tag{4}$$

where unit quaternion $\boldsymbol{q} = [\eta\ \boldsymbol{\epsilon}]^T$. The symbol $^\times$ denotes that the vector is on the *skew symmetric form*, defined in [11].

B. Navigation Equations

The navigation equations are derived in [9] by using a matrix differential equation to represent the attitude. In [12] the matrix differential equation is transformed into a four dimensional differential equation using quaternions. All the derivation of the states are made in the inertial frame, and then the states are transformed to the wanted frames. The navigation equations are given below

$$\begin{aligned} \dot{\boldsymbol{v}}^l =& \boldsymbol{R}(\boldsymbol{q}_b^l)\boldsymbol{f}^b + \bar{\boldsymbol{g}}^l - \\ & ((\boldsymbol{\omega}_{il}^l)^\times + (\boldsymbol{R}_e^l(\phi, \lambda)\boldsymbol{\omega}_{ie}^e)^\times)\boldsymbol{v}^l \end{aligned} \tag{5a}$$

$$\dot{\boldsymbol{p}}^e = \boldsymbol{R}_l^e(\phi, \lambda)\boldsymbol{v}^l \tag{5b}$$

$$\dot{\boldsymbol{q}}_b^l = \left(\bar{\boldsymbol{\Omega}}(\boldsymbol{\omega}_{ib}^b) - \boldsymbol{\Omega}(\boldsymbol{\omega}_{il}^l)\right)\boldsymbol{q}_b^l \tag{5c}$$

Equation (5a) is the time derivative of the velocity $\boldsymbol{v}^l$ represented in the local-level frame. The right side of the equation has three terms. The first term is the force working on the object. This term consists of the measured force from accelerometers $\boldsymbol{f}^b$ in the body frame and the coordinate transformation matrix $\boldsymbol{R}(\boldsymbol{q}_b^l)$ which transforms the force to the local-level frame. The coordinate transformation matrix is calculated from the quaternion $\boldsymbol{q}_b^l$ using (4). The second term is the gravity force, which include both the force generated by the attraction of mass and the centrifugal acceleration. A gravity model shall be shown in the next section. The third and last term is forces generated by a rotating earth. $\boldsymbol{\omega}_{il}^l$ is the angular velocity of inertial frame with respect to local-level frame represented in local-level frame, and will be defined in the next section. $\boldsymbol{\omega}_{ie}^e$ is the angular velocity of earth frame with respect to inertial frame represented in earth frame. This velocity is given in the WGS-84 parameters given in [8]. This vector is transformed to the local-level frame by the coordinate transformation matrix $\boldsymbol{R}_e^l(\phi, \lambda)$, which is the transposition of the matrix found in (2).

Equation (5b) is the time derivative of the position $\boldsymbol{p}^e$, represented in the earth frame. This is equal the velocity $\boldsymbol{v}^l$ in the local-level frame transformed into the earth frame by using the coordinate transformation matrix $\boldsymbol{R}_l^e$ found in (2). Equation (5c) is the time derivative of the unit quaternion, which represents the attitude between the body frame and the local-level frame, hence the super- and subscript. $\boldsymbol{\omega}_{il}^l$ is the angular velocity of the inertial frame, as above. $\boldsymbol{\omega}_{ib}^b$ is the angular velocity of the inertial frame with respect to the body frame, represented in the body frame. This speed is measured by the gyroscopes. The functions $\boldsymbol{\Omega}(\boldsymbol{\omega})$ and $\bar{\boldsymbol{\Omega}}(\boldsymbol{\omega})$ transform the rotation speed to be used in the quaternion differential equation and are defined as:

$$\boldsymbol{\Omega}(\boldsymbol{\omega}) = \frac{1}{2}\begin{bmatrix} 0 & -\boldsymbol{\omega}^T \\ \boldsymbol{\omega} & \boldsymbol{\omega}^\times \end{bmatrix} \quad \bar{\boldsymbol{\Omega}}(\boldsymbol{\omega}) = \frac{1}{2}\begin{bmatrix} 0 & -\boldsymbol{\omega}^T \\ \boldsymbol{\omega} & -\boldsymbol{\omega}^\times \end{bmatrix} \tag{6}$$

1) Gravity Model: To compensate for the gravity we need an accurate gravity model. The model presented below is found in [8]. The gravity normal to the ellipsoid is γ given by

$$\gamma(\phi) = \gamma_e \frac{1 + k\sin^2\phi}{\sqrt{1 - e^2\sin^2\phi}} \tag{7}$$

where ϕ is the latitude, k is

$$k = \frac{b\gamma_p}{a\gamma_e} - 1 \tag{8}$$

and e^2, γ_e, γ_p, a and b is WGS-84 parameters. When the object is above the surface of the ellipsoid the gravity vector will be slightly off the normal to the ellipsoid. This will produce a gravity component along the north direction. For a point h meters above the mean sea level the downward component of the normal gravity is

$$\gamma_h(\phi, h) = \gamma(\phi)\left(1 - \tfrac{2}{a}\left(1 - f + m - 2f\sin^2\phi\right)h\right) \tag{9}$$

where a, f, m is WGS-84 parameters and ϕ is the latitude. The north component is

$$\gamma_n(\phi, h) = -8,08 \cdot 10^{-6} h \sin(2\phi) \tag{10}$$

In vector form the normal gravity is

$$\boldsymbol{\gamma}^l = [0\ \ \gamma_n(\phi, h)\ \ -\gamma_h(\phi, h)]^T \tag{11}$$

This replaces the gravity vector $\bar{\boldsymbol{g}}^l$ in the system (5) with $\boldsymbol{\gamma}^l$.

2) Rotation Speed Between the Inertial Frame and the Local-Level Frame: The rotation speed between the inertial frame and the local-level frame $\boldsymbol{\omega}_{il}^{l}$ is [8], [10]

$$\boldsymbol{\omega}_{il}^{l} = \begin{bmatrix} -\dot{\phi} & (\dot{\lambda} + \omega_{ie})\cos\phi & (\dot{\lambda} + \omega_{ie})\sin\phi \end{bmatrix}^T \tag{12}$$

where ω_{ie} is the earth rotation speed found in WGS-84, λ is the longitude and ϕ is the latitude.

It can be showed that (12) can be written as [8]

$$\boldsymbol{\omega}_{il}^{l} = \begin{bmatrix} -\frac{v_n}{R_m+h} \\ \frac{v_e}{R_p+h} + \omega_{ie}\cos\phi \\ \frac{v_e \tan\phi}{R_p+h} + \omega_{ie}\sin\phi \end{bmatrix} \tag{13}$$

where R_m is the meridian radius of the curvature, R_p is the prime radius of curvature, v_n is the velocity in the north direction and v_e is the velocity in the east direction. Now all components in the system (5) are well defined and it is possible to use the system to calculate the position to an object.

C. Initialization of the Navigation Equations

In order to calculate the position based on sensor measurements we also need to know the initial state in the navigation equations (5). In this article we assume zero velocity when the system starts. The initial position is obtained by a GPS on the test unit. The initial attitude is obtained by using accelerometer and magnetometer measurements, which are two vectors in the body frame. By comparing these two vectors with the corresponding vectors in the local-level frame it is possible to calculate the initial attitude using the QUEST algorithm[13]. The accelerometer measurement vector is compared with the gravitation model (11). The magnetometer measurement vector is compared with 11th generation International Geomagnetic Reference Field (IGRF) model[14], which is a model of the earth magnetic field.

1) The QUEST Algorithm: The QUEST algorithm is an optimal algorithm which determines the attitude from an arbitrary number of vectors. The algorithm seeks to satisfy the equations [13]

$$\boldsymbol{A}\hat{\boldsymbol{v}}_i = \hat{\boldsymbol{w}}_i \qquad i = 1, \cdots, n \tag{14}$$

where A is an orthogonal matrix (the attitude matrix), $\hat{\boldsymbol{v}}_1, \cdots, \hat{\boldsymbol{v}}_n$ is a set of reference unit vectors in the reference coordinate system, $\hat{\boldsymbol{w}}_1, \cdots, \hat{\boldsymbol{w}}_n$ is a set of observation unit vectors in the body coordinate system and n is the number of vectors. The Quest algorithm minimizes the loss function

$$L(\boldsymbol{A}) = \frac{1}{2}\sum_{i=1}^{n} a_i |\hat{\boldsymbol{w}}_i - \boldsymbol{A}\hat{\boldsymbol{v}}_i|^2 \tag{15}$$

Introducing the quantities

$$\boldsymbol{B} = \sum_{i=1}^{n} a_i \hat{\boldsymbol{w}}_i \hat{\boldsymbol{v}}_i^T \qquad \boldsymbol{z} = \sum_{i=1}^{n} a_i (\hat{\boldsymbol{w}}_i \times \hat{\boldsymbol{v}}_i) \tag{16}$$

the problem can be reduced to maximize the function

$$g(\boldsymbol{q}) = \boldsymbol{q}^T \boldsymbol{K} \boldsymbol{q} \qquad \text{subject to } \boldsymbol{q}^T\boldsymbol{q} = 1 \tag{17}$$

where

$$\boldsymbol{K} = \begin{bmatrix} \boldsymbol{B} + \boldsymbol{B}^T - (tr\boldsymbol{B})\boldsymbol{I} & \boldsymbol{z} \\ \boldsymbol{z}^T & tr\boldsymbol{B} \end{bmatrix} \tag{18}$$

It can be shown that

$$\boldsymbol{K}\bar{\boldsymbol{q}}_{opt} = \lambda_{max}\bar{\boldsymbol{q}}_{opt} \tag{19}$$

This means that the optimal quaternion is the eigenvector for the largest eigenvalue of $\boldsymbol{K}$ [13].

D. Unscented Kalman Filter

In many applications the Kalman filter can not be used because the system is nonlinear. The nonlinear system in the discrete case can be written as

$$\boldsymbol{x}_{k+1} = \boldsymbol{f}_k(\boldsymbol{x}_k, \boldsymbol{v}_k, \boldsymbol{u}_k) \tag{20a}$$
$$\boldsymbol{z}_k = \boldsymbol{h}_k(\boldsymbol{x}_k, \boldsymbol{w}_k) \tag{20b}$$

where the following assumptions are made

$$E[\boldsymbol{x}_0] = \bar{\boldsymbol{x}}_0 \quad E[\boldsymbol{x}_0\boldsymbol{v}_k^T] = \boldsymbol{0} \quad E[\delta\boldsymbol{x}_0\delta\boldsymbol{x}_0^T] = \bar{\boldsymbol{P}}_0 \tag{21a}$$
$$E[\boldsymbol{v}_k] = \boldsymbol{0} \quad E[\boldsymbol{x}_0\boldsymbol{w}_k^T] = \boldsymbol{0} \quad E[\boldsymbol{v}_k\boldsymbol{v}_l^T] = \delta_{kl}\boldsymbol{Q}_k \tag{21b}$$
$$E[\boldsymbol{w}_k] = \boldsymbol{0} \quad E[\boldsymbol{v}_k\boldsymbol{w}_l^T] = \boldsymbol{0} \quad E[\boldsymbol{w}_k\boldsymbol{w}_l^T] = \delta_{kl}\boldsymbol{R}_k \tag{21c}$$

where $\delta\boldsymbol{x}_0 = \boldsymbol{x}_0 - \bar{\boldsymbol{x}}_0$, $\boldsymbol{x}$ is the state vector, $\boldsymbol{v}$ is the process noise vector, $\boldsymbol{u}$ is the control input vector, $\boldsymbol{w}$ is the measurement noise vector and $\boldsymbol{z}$ is the measurements.

The *unscented Kalman filter* (UKF) is based on the principle that it is easier to approximate the probability density functions than the nonlinear functions. This is achieved by using the *Scaled Unscented transform*[15], [16], which guarantees that the mean and covariance has a second order accuracy.

A set of *sigma points* is selected so that the points have the same mean and covariance as the underlying distribution, which is $\bar{\boldsymbol{x}}$ and $\boldsymbol{P}_{xx}$. If the random variable has dimension L then $2L+1$ points are selected by the following scheme[15]

$$\mathcal{W}_0 = \boldsymbol{0} \tag{22}$$
$$\mathcal{W}_i = \left(\sqrt{(L+\lambda)\boldsymbol{P}_{xx}}\right)_i \qquad \forall\ i \in [1, L] \tag{23}$$
$$\mathcal{W}_i = -\left(\sqrt{(L+\lambda)\boldsymbol{P}_{xx}}\right)_{i-L} \qquad \forall\ i \in [L+1, 2L] \tag{24}$$

And the sigma points $\mathcal{X}_i$ are created by

$$\mathcal{X}_i = \bar{\boldsymbol{x}} + \mathcal{W}_i \qquad \forall\ i \in [0, 2L] \tag{25}$$

These sigma points have corresponing weights, which will be used when calculating the mean and covariance. These weights are defined as

$$W_0^m = \lambda/(L+\lambda) \tag{26}$$
$$W_0^c = \lambda/(L+\lambda) + (1 - \alpha^2 + \beta) \tag{27}$$
$$W_i^m = W_i^c = 1/\left((2(L+\lambda)\right) \qquad \forall\ i \in [1, 2L] \tag{28}$$

where $\lambda = \alpha^2(L+\kappa) - L$ is a scaling parameter. The constants α, β and κ are parameters that can be used to optimize the transform. Prior knowledge about the distribution is given to the transform by the constant β. For Gaussian distributions $\beta = 2$ is optimal[16]. The spread of the sigma points around

$\bar{\boldsymbol{x}}$ is determined by the constant α, which is set to a small positive value. κ is a secondary scaling parameter which is set to zero by [15]. $\boldsymbol{\mathcal{X}}$ is a matrix with $2L+1$ sigma vectors $\mathcal{X}_i$. All these vectors are used as inputs to the nonlinear function to produce the transformed sigma points $\boldsymbol{\mathcal{Y}} = [\mathcal{Y}_0 \ \cdots \ \mathcal{Y}_{2L}]$

$$\mathcal{Y}_i = \boldsymbol{f}(\mathcal{X}_i) \ \ \forall \ i \in [0, 2L] \tag{29}$$

The mean is given by the weighted average

$$\bar{\boldsymbol{y}} = \sum_{i=0}^{2L} W_i^m \mathcal{Y}_i \tag{30}$$

The covariance is given by the weighted outer product

$$\boldsymbol{P}_{yy} = \sum_{i=0}^{2L} W_i^c (\mathcal{Y}_i - \bar{\boldsymbol{y}})(\mathcal{Y}_i - \bar{\boldsymbol{y}})^T \tag{31}$$

1) Using the Unscented Kalman Filter with Quaternions: Since the quaternion in the state vector $\bar{\boldsymbol{x}}$ is not a member of a vector space, but a member of a *homogeneous Riemannian manifold* (the four dimensional unit sphere) (30) will not yield the correct result. We will use the method described in [17] to avoid this problem.

The set $\{\mathcal{W}_i\}$ is calculated as in (22), but the sigma points of (25) is calculated in another manner. First we divide the set $\{\mathcal{W}_i\}$ into two parts. One part containing the vectors for the quaternions $\mathcal{W}_i^q$ and another part $\mathcal{W}_i^o$ containing all the other vectors. The dimention of $\mathcal{W}_i^q$ is $\mathbb{R}^3$ and are considered rotation vectors. This can be written as

$$\mathcal{W}_i = \begin{bmatrix} \mathcal{W}_i^o & \mathcal{W}_i^q \end{bmatrix}^T \tag{32}$$

From the set $\{\mathcal{W}_i^q\}$ we create a noise quaternion that rotates the quaternion in the state vector, thus ensures that all the quaternions in the sigma points is unit quaternions. We transforms the rotation vectors in $\{\mathcal{W}_i^q\}$ to angle-axis parameters

$$\theta_i = |\mathcal{W}_i^q| \qquad \boldsymbol{k}_i = \mathcal{W}_i^q / |\mathcal{W}_i^q| \tag{33}$$

And creates a quaternion from the angle-axis parameters with

$$\boldsymbol{q}_{\mathcal{W}_i^q} = \left[\cos\left(\tfrac{\theta_i}{2}\right) \ \ \boldsymbol{k}_i \sin\left(\tfrac{\theta_i}{2}\right)\right]^T \tag{34}$$

If $\mathcal{W}_i^q = \boldsymbol{0}$ we have a singularity in $\boldsymbol{k}_i$. When the rotation vector is zero we have no rotation and sets $\boldsymbol{q}_{\mathcal{W}_i^q} = [1 \ 0 \ 0 \ 0]^T$ to avoid the singularity. The sigma points is created by using

$$\mathcal{X}_i = \begin{bmatrix} \bar{\boldsymbol{x}}^o + \mathcal{W}_i^o & \bar{\boldsymbol{q}} \otimes \boldsymbol{q}_{\mathcal{W}_i^q} \end{bmatrix}^T \tag{35}$$

where $\otimes$ represents the *quaternion product*.

The sigma points are used as inputs for the nonlinear function in the same manner as in (29), but the mean cannot be calculated as in (30) because the resulting quaternion might not be a unit quaternion. Therefor $\mathcal{Y}_i$ is divided in the same manner as in (32) and the iterative method found in [17] is used to estimate the mean quaternion $\bar{\boldsymbol{q}}_{\mathcal{Y}}$ of $\mathcal{Y}_i^q$.

The covariance of the sigma points is calculated by squaring the sigma point subtracted with the mean, as in (31). For the quaternions the error can not be found by subtraction, but by finding the error quaternion defined by

$$\boldsymbol{e}_i = \boldsymbol{q}_{\mathcal{Y}_i} \otimes \bar{\boldsymbol{q}}_{\mathcal{Y}}^{-1} \tag{36}$$

In order to calculate the covariance of sigma points $\{\mathcal{Y}_i\}$ we need to convert the quaternions back to rotation vectors. This is done reversing the method in (33) and (34), this yields

$$\theta_i = 2\cos^{-1} Re(\boldsymbol{e}_i) \qquad \boldsymbol{r}_i = Im(\boldsymbol{e}_i)\theta_i \tag{37}$$

We can now calculate the covariance with by

$$\boldsymbol{P}_{yy} = \sum_{i=0}^{2L} W_i^c \mathcal{W'}_i \mathcal{W'}_i^T \tag{38}$$

where $\mathcal{W'}_i$ is the error and is defined by

$$\mathcal{W}_i' = \begin{bmatrix} \mathcal{W}_i^o - \bar{\boldsymbol{y}}^o & \boldsymbol{r}_i \end{bmatrix}^T \tag{39}$$

The cross correlation matrix is calculated according to

$$\boldsymbol{P}_{xz} = \sum_{i=0}^{2L} W_i^c \mathcal{W'}_i (\mathcal{Z}_i - \boldsymbol{z})^T \tag{40}$$

The Kalman gain found with the normal UKF equation and the correction to the predicted value is defined $\tilde{\boldsymbol{x}}$ as

$$\delta\tilde{\boldsymbol{x}}_k = \boldsymbol{K}_k(\boldsymbol{z}_k - \bar{\boldsymbol{z}}_k) \tag{41}$$

where $\boldsymbol{z}_k$ is the actual measure and $\bar{\boldsymbol{z}}_k$ is the predicted measure obtained from the measurement update equation. Since the correction $\delta\tilde{\boldsymbol{x}}_k$ contains the rotation vector, and not the quaternion we must transform the rotation vector to a quaternion $\boldsymbol{q}_z$ in the same manner as in (34). The correction $\delta\tilde{\boldsymbol{x}}_k$ is divided into two parts, $\delta\tilde{\boldsymbol{x}}_k^q$ contains the rotaion vector and $\delta\tilde{\boldsymbol{x}}_k^o$ contains the other states. $\delta\tilde{\boldsymbol{x}}_k^q$ is used to create $\boldsymbol{q}_z$. The update from the prediction $\tilde{\boldsymbol{x}}_k$ to the estimate $\hat{\boldsymbol{x}}_k$ is

$$\hat{\boldsymbol{x}}_k = \begin{bmatrix} \tilde{\boldsymbol{x}}_k^o + \delta\tilde{\boldsymbol{x}}_k^o & \tilde{\boldsymbol{q}}_k \otimes \boldsymbol{q}_z \end{bmatrix}^T \tag{42}$$

The covariance is updated using the normal UKF equations.

E. Converting Sensor Data to Navigation Information

This section describes how to convert pressure information to altitude information and magnetic field data into attitude information.

1) Pressure to Altitude: It is possible to use a pressure sensor as an altimeter[18]. The US Standard Atmosphere 1976 is an approximation of the atmosphere. For land based navigation, the pressure model for the troposphere is used, which is

$$p = P_0 \left(1 - h\frac{T_{grad}}{T_0}\right)^{\frac{g}{R \cdot T_{grad}}} \tag{43}$$

where p is pressure, h is height above sea level, P_0 is zero altitude pressure, T_0 is zero altitude temperature which is 288.15 K, T_{grad} is the temperature gradient in the troposphere which is $6.5 \cdot 10^{-3}$ K/m, R is the specific gas constant which is 287.052 J/(K·kg) and g is the gravity constant. The function do not take special weather conditions into account. Neither that the pressure changes with the weather. To compensate for

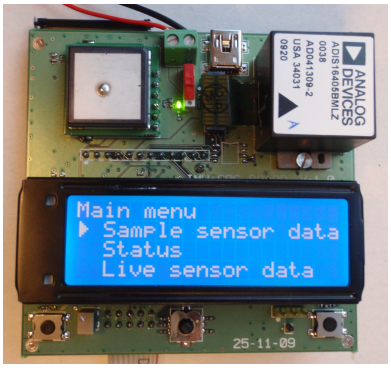

Fig. 1. The test unit

pressure changes due to weather one can calibrate the zero altitude pressure by the following formula

$$P_{0,cal}(h_0, p_0) = \frac{p_0}{\left(1 - h_0 \frac{T_{grad}}{T_0}\right)^{\frac{g}{R \cdot T_{grad}}}} \tag{44}$$

where $P_{0,cal}$ is the calibrated zero altitude pressure, h_0 is the known altitude and p_0 is the pressure at this altitude.

2) Earth's Magnetic Field: We will use the International Geomagnetic Reference Field (IGRF) model [14] as our earth's magnetic field model. The latest IGRF model is the 11th generation [19]. The IGRF-11 model implementation used in this article is obtained from [20]. This program returns the magnetic field in the local-level frame and it is possible to compare this with the measured field in the body frame to improve the attitude estimation.

[21] contains guidelines for using the IGRF model and warns about using the IGRF model near the earth's surface because of small fields created by for instance cars, buildings and magnetization of crustal rocks. In addition natural fields from electric currents in the ionosphere and magnetic storms will also contribute to the error. A root mean square error of approximately 200 nT is mentioned. It is also stated that the error could be much larger, hence we will use an RMS error 800 nT as an approximation of the model error.

III. Test Unit

We have developed a test unit that collects data from a GPS, gyroscopes, accelerometers, magnetometers and a barometer. The development is documented in [22], [12]. The GPS is a UP500 from Fastrax [23]. This unit has an accuracy of 1.8 m measured in CEP95. The gyroscopes, accelerometers and magnetometers are all inside a ADIS16405 from Analog devices [24]. The gyroscopes has a angel random walk coefficient of 2.0 $^\circ/\sqrt{\text{hr}}$ and a bias instability coefficient of 0.007 $^\circ$/s. The accelerometer has a noise density of 8.66 mg and the magnetometer has a noise density of 2.59 mgauss. The barometer is a MS5534C from Intersema [25]. The datasheet does not specify a noise density. The data is sampled and saved on a SD card. Fig. 1 shows the test unit.

IV. Modeling

In this section we create models to be used with the UKF. We will use the subscripts GPS for GPS, gy for gyroscope, ac for accelerometer, ma for magnetometer and ba for barometer.

A. Sensor Error Modeling

In this section we will create sensor models for the GPS, gyroscope, accelerometer, magnetometer and barometer.

1) GPS: Dilution of precision (DOP) is a number that characterizes the satellite geometry. If the satellites are spread out in the sky the GPS will produce a better estimate than if the satellites where close together[26].

The error in the position estimate from the GPS has many sources. Error in the satellite clock, signal delay in the ionosphere and atmosphere and multi-path is some of the error sources. If we assume that these errors can be reduced to a single constant σ_{UERE}, which is known as the total *user equivalent range error*. We also assume that the error is equal in all directions and over all observation. The different DOP values may be represented as a function of σ_{UERE} [26]

$$HDOP = \frac{\sqrt{\sigma_E^2 + \sigma_N^2}}{\sigma_{UERE}} \qquad VDOP = \frac{\sqrt{\sigma_U^2}}{\sigma_{UERE}} \tag{45}$$

where σ_E^2, σ_N^2, σ_U^2 is the variance in the east, north and upward direction of the position estimate. HDOP is the *horizontal* DOP, VDOP is the *vertical* DOP. Because the DOP values are a function of the position of the GPS receiver and the satellites these values can be predicted by using an almanac over the GPS satellites.

We assume that the variance in the north and east directions are equal, renaming both to the horizontal variance σ_H^2. We also rename the variance in the upward direction σ_U^2 to variance in the vertical direction σ_V^2. Inserting these properties into (45) and solving the equations yields

$$\sigma_H^2 = \tfrac{1}{2} HDOP^2 \sigma_{UERE}^2 \qquad \sigma_V^2 = VDOP^2 \sigma_{UERE}^2 \tag{46}$$

This results in a covariance matrix for the position obtained by the GPS given below

$$\boldsymbol{P}_{GPS}^l = diag(\sigma_H^2, \sigma_H^2, \sigma_V^2) \tag{47}$$

The $diag(\cdot)$ function creates a diagonal matrix if the inputs are scalars, with the inputs on the main diagonal of the matrix. If the inputs are matrices a block-diagonal matrix is created with the blocks on the main diagonal. The following formula transforms $\boldsymbol{P}_{GPS}^l$ into the earth frame.

$$\boldsymbol{P}_{GPS}^e = \boldsymbol{R}_l^e(\phi, \lambda) \boldsymbol{P}_{GPS}^l (\boldsymbol{R}_l^e(\phi, \lambda))^T \tag{48}$$

2) Gyroscope: A general error model for gyroscopes is found in [27]. The g-sensitive bias is low, according to the datasheet for ADIS16400[24], and is therefore omitted. This results in the error model

$$\tilde{\boldsymbol{\omega}} = (\boldsymbol{I} + \boldsymbol{S}_{gy})\boldsymbol{\omega} + \boldsymbol{M}_{gy}\boldsymbol{\omega} + \boldsymbol{b}_{gy} + \boldsymbol{n}_{gy} \tag{49}$$

where $\tilde{\boldsymbol{\omega}}$ is the measurement and $\boldsymbol{\omega}$ is the true value. Calibration constants are *scale-factor error* ($\boldsymbol{S}_{gy}$), *cross-coupling* ($\boldsymbol{M}_{gy}$), *g-insensitive bias* ($\boldsymbol{b}_{gy}$) and noise ($\boldsymbol{n}_{gy}$).

The noise $\boldsymbol{n}_{gy}$ is modeled by using Allan variance parameters[28]. We use the *Angle Random Walk* coefficient N and the *Bias Instability* coefficient B. For the three dimensional system the noise is modeled as

$$\boldsymbol{n}_{gy}[k] = \boldsymbol{n}_{gy,w}[k] + \boldsymbol{n}_{gy,p}[k] \tag{50a}$$

$$\boldsymbol{n}_{gy,p}[k+1] = e^{-T\boldsymbol{\beta}}\boldsymbol{n}_{gy,p}[k] + \boldsymbol{n}_{p,w}[k] \tag{50b}$$

Both $\boldsymbol{n}_{gy,w}$ and $\boldsymbol{n}_{p,w}$ are white noise sequences, and T is the sample time. The white noise $\boldsymbol{n}_{gy,w}$ has a covariance of

$$\boldsymbol{\Sigma}_{gy,w} = T^{-1} diag(N_x^2, N_y^2, N_z^2) \tag{51}$$

where N_i is the Angle Random Walk coefficient for the ith axis and T is the sample time. The white noise process $\boldsymbol{v}_{p,w}$ has a covariance of

$$\boldsymbol{\Sigma}_{p,w} = \tfrac{1}{2}\boldsymbol{\Phi}_{p,w}(\boldsymbol{I} - e^{-T\boldsymbol{\beta}}) \tag{52}$$

where $\boldsymbol{\Phi}_{p,w}$ is the power spectral density of the corresponding continuous Gauss-Markov process, which is [12]

$$\boldsymbol{\Phi}_{p,w}[i,j] = \begin{cases} \frac{B_i^2 S_{m,i}}{2\sqrt{N_i^2(S_{m,i}-N_i^2)}} & \forall\ i = j \\ 0 & \forall\ i \neq j \end{cases} \tag{53}$$

where B_i is the Bias Instability coefficient for the ith axis. The inverse of the time constant is given by [12]

$$\boldsymbol{\beta}[i,j] = \begin{cases} \frac{B_i^2}{N_i^2}\sqrt{\frac{N_i^2}{S_{m,i}-N_i^2}} & \forall\ i = j \\ 0 & \forall\ i \neq j \end{cases} \tag{54}$$

$S_{m,i}$ is the power spectral density for the Gauss-Markov process when the frequency is zero. This should ideally be equal to infinity in order to model flicker noise perfectly, but is set to a high value as an approximation. We use $S_{m,i} = 10$.

3) Accelerometer: The accelerometer are subject to the following error source according to [27], *g-indepented bias* ($\boldsymbol{b}_{ac}$), *scale factor error* ($\boldsymbol{S}_{ac}$), *cross coupling error* ($\boldsymbol{M}_{ac}$) and *vibro-pendulous error*. We are unable to calibrate the vibro-pendulous error because of lack of equipment. This reduces the error model to

$$\tilde{\boldsymbol{a}} = (\boldsymbol{I} + \boldsymbol{S}_{ac})\boldsymbol{a} + \boldsymbol{M}_{ac}\boldsymbol{a} + \boldsymbol{b}_{ac} + \boldsymbol{n}_{ac} \tag{55}$$

where $\tilde{\boldsymbol{a}}$ is the measurements and $\boldsymbol{a}$ is the true value. The noise vector $\boldsymbol{n}_{ac}$ has a covariance matrix $\boldsymbol{\Sigma}_{ac}$.

4) Magnetometer: The error model for the magnetometer is similar to the gyroscope and accelerometer case and is postulated to be

$$\tilde{\mathbf{B}} = (\boldsymbol{I} + \boldsymbol{S}_{ma})\mathbf{B} + \boldsymbol{b}_{ma,f} + \boldsymbol{n}_b \tag{56}$$

where $\tilde{\mathbf{B}}$ is the measured magnetic field, $\boldsymbol{S}_{ma}$ is the scale factor error, $\mathbf{B}$ is the true magnetic field, $\boldsymbol{b}_{ma,f}$ is the bias and $\boldsymbol{n}_b$ is white noise with a covariance matrix $\boldsymbol{\Sigma}_{ma}$.

5) Barometer: The sensor MS5534C measure both pressure and temperature. The datasheet [25] describes an algorithm to compensate for temperature error and also loads factory calibration constants, which is implemented on the test unit. With this compensation it is reasonable to assume that the sensor produces small errors. Therefore we postulate the following model with only scale-factor error, bias and noise

$$\tilde{p} = (1 + S_{ba})p + B_{ba,f} + n_{ba} \tag{57}$$

The noise term n_{ba} is assumed to be white noise with a covariance of Σ_{ba}.

6) Calibration: All the sensors except the magnetometers has been calibrated accurately, because of lack of a calibration equipment for the magnetometer. The calibration results are given in [12]. All the sensors was mounted on the PCB when they where calibrated. The magnetometers has been calibrated on a gyro rate board. The rate board contains a lot of magnetic materials, making the calibration inaccurate. In the real world test the sensor was mounted on the rate board, thus the magnetometer should be fairly accuratly calibrated in the real world test.

B. Positioning with Inertial Sensors

We now want to find the process equation for the system with only inertial sensors on the form

$$\boldsymbol{x}_k = \boldsymbol{f}_k(\boldsymbol{x}_k, \boldsymbol{v}_k, \boldsymbol{u}_k) \tag{58}$$

The process equation is obtained by using Euler's method on (5). This equation includes both the accelerometer output and the gyroscope output as a control input vector $\boldsymbol{u}_k$, making $\boldsymbol{u}_k = [(\tilde{\boldsymbol{a}}^b[k])^T\ (\tilde{\boldsymbol{\omega}}_{ib}^b[k])^T]^T$ The equations for the calibrated output from the accelerometer and gyroscope can by simple manipulations of (55) and (49) be written as

$$\boldsymbol{a} = (\boldsymbol{I} + \boldsymbol{S}_{ac} + \boldsymbol{M}_{ac})^{-1}(\tilde{\boldsymbol{a}} - \boldsymbol{b}_{ac,f} - \boldsymbol{n}_{ac}) \tag{59}$$

$$\boldsymbol{\omega} = (\boldsymbol{I} + \boldsymbol{S}_{gy} + \boldsymbol{M}_{gy})^{-1}(\tilde{\boldsymbol{\omega}} - \boldsymbol{b}_{gy,f} - \boldsymbol{n}_{gy}) \tag{60}$$

where $\tilde{\boldsymbol{a}}$ is the measured acceleration, $\boldsymbol{a}$ is the true acceleration, $\tilde{\boldsymbol{\omega}}$ is the measured angular velocity, $\boldsymbol{\omega}$ is the true angular velocity, $\boldsymbol{n}_{ac}$ and $\boldsymbol{n}_{gy}$ are noise. The coefficients are described in Section IV-A. By scaling the noise and dividing the gyro noise into a white noise part and a $1/f$ noise part we get

$$\boldsymbol{a} = \boldsymbol{E}_{ac}^{-1}(\tilde{\boldsymbol{a}} - \boldsymbol{b}_{ac,f}) + \boldsymbol{v}_{ac} \tag{61}$$

$$\boldsymbol{\omega} = \boldsymbol{E}_{gy}^{-1}(\tilde{\boldsymbol{\omega}} - \boldsymbol{b}_{gy,f}) + \boldsymbol{v}_{gy,w} - \boldsymbol{v}_{gy,p} \tag{62}$$

where $\boldsymbol{v}_{ac}$ and $\boldsymbol{v}_{gy,w}$ is the scaled white noise, $\boldsymbol{v}_{gy,p}$ is the scaled $1/f$ noise, $\boldsymbol{E}_{ac} = \boldsymbol{I} + \boldsymbol{S}_{ac} + \boldsymbol{M}_{ac}$ and $\boldsymbol{E}_{gy} = \boldsymbol{I} + \boldsymbol{S}_{gy} + \boldsymbol{M}_{gy}$. When we calibrated the gyroscopes we ignored the earth rotation because it is much smaller than the noise generated by the gyroscopes, therefore we can remove $\boldsymbol{\omega}_{il}^l$ from equation (5c). We want to use the noise model found in Section IV-A2, and therefor we augment (5) with three states. Inserting (61)

and (62) into the process equation (5) and augmenting yields

$$\begin{aligned}\boldsymbol{v}^l[k{+}1] =& T\boldsymbol{R}_b^l(\boldsymbol{E}_{ac}^{-1}(\tilde{\boldsymbol{a}}^b[k]-\boldsymbol{b}_{ac,f}^b)+\boldsymbol{v}_{ac}^b)+T\boldsymbol{\gamma}^l[k]+\\ &(\boldsymbol{I}-T((\boldsymbol{\omega}_{il}^l)^\times-(\boldsymbol{R}_e^l\boldsymbol{\omega}_{ie}^e)^\times))\boldsymbol{v}^l[k] \quad (63a)\\ \boldsymbol{p}^e[k{+}1] =& \boldsymbol{p}^e[k]+T\boldsymbol{R}_l^e\boldsymbol{v}^l[k] \quad (63b)\\ \boldsymbol{q}_b^l[k{+}1] =& \Big(\boldsymbol{I}+T\big(\bar{\boldsymbol{\Omega}}(\boldsymbol{E}_{gy}^{-1}(\tilde{\boldsymbol{\omega}}_{ib}^b[k])-\boldsymbol{b}_{gy,f}^b)+\\ &\bar{\boldsymbol{\Omega}}(\boldsymbol{v}_{gy,w}^b-\boldsymbol{v}_{gy,p}^b)\big)\Big)\boldsymbol{q}_b^l[k] \quad (63c)\\ \boldsymbol{v}_{gy,p}^b[k{+}1] =& e^{-T\boldsymbol{\beta}}\boldsymbol{v}_{gy,p}^b[k]+\boldsymbol{v}_{p,w}^b[k] \quad (63d)\end{aligned}$$

The equation (63) is denoted $\boldsymbol{f}_{INS}(\boldsymbol{x}_k,\boldsymbol{v}_k,\boldsymbol{u}_k)$.

The new state vector, the initial expectation value of the new state vector and the new noise vector are

$$\boldsymbol{x}_k=\begin{bmatrix}\boldsymbol{v}^l[k]\\ \boldsymbol{p}^e[k]\\ \boldsymbol{q}_b^l[k]\\ \boldsymbol{v}_{gy,p}^b[k]\end{bmatrix}\quad \bar{\boldsymbol{x}}_0=\begin{bmatrix}\bar{\boldsymbol{v}}^l[0]\\ \bar{\boldsymbol{p}}^e[0]\\ \bar{\boldsymbol{q}}_b^l[0]\\ \bar{\boldsymbol{v}}_{gy,p}^b[0]\end{bmatrix}\quad \boldsymbol{v}_k=\begin{bmatrix}\boldsymbol{v}_{ac}^b[k]\\ \boldsymbol{v}_{gy,w}^b[k]\\ \boldsymbol{v}_{p,w}^b[k]\end{bmatrix}$$

where $\bar{\boldsymbol{p}}^e[0]$ is obtained from the GPS, $\bar{\boldsymbol{v}}^l[0]$ is set to zero and it is assumed that the test unit is stationary when starting up. $\bar{\boldsymbol{q}}_b^l[0]$ is obtained from the QUEST algorithm and $\bar{\boldsymbol{v}}_{gy,p}^b[0]=\boldsymbol{0}$. This leads to the initial covariance of the system to be

$$\bar{\boldsymbol{P}}_0=diag(\boldsymbol{0},\boldsymbol{P}_{GPS}^e,\boldsymbol{P}_{q,0},\boldsymbol{0}) \quad (64)$$

where $\boldsymbol{P}_{GPS}^e$ is obtained from the GPS in (48) and $\boldsymbol{P}_{q,0}$ is obtained from the QUEST algorithm. The noise covariance is

$$\boldsymbol{Q}_{INS}=diag(\boldsymbol{Q}_{ac},\boldsymbol{Q}_{gy,w},\boldsymbol{Q}_{p,w}) \quad (65)$$

where $\boldsymbol{Q}_{ac}$ is the noise from the accelerometer, $\boldsymbol{Q}_{gy,w}$ is the white noise from the gyroscopes and $\boldsymbol{Q}_{p,w}$ is the white noise for $1/f$ noise approximation. These can be found from

$$\boldsymbol{Q}_{ac}=T\boldsymbol{E}_{ac}^{-1}\boldsymbol{\Sigma}_{ac}\boldsymbol{E}_{ac}^{-T} \quad (66)$$

$$\boldsymbol{Q}_{gy,w}=\boldsymbol{E}_{gy}^{-1}\boldsymbol{\Sigma}_{gy,w}\boldsymbol{E}_{gy}^{-T} \quad (67)$$

$$\boldsymbol{Q}_{p,w}=\boldsymbol{E}_{gy}^{-1}\boldsymbol{\Sigma}_{p,w}\boldsymbol{E}_{gy}^{-T} \quad (68)$$

where T is the sampling time. We have now found the necessary functions and coefficients in order to use the UKF.

1) Filtering Gyro Output: To remove some of the flicker noise from the gyroscope measurements we used a 10. order high pass IIR Butterworth filter[12]. When filtering the gyroscope output the flicker noise of equation (63) can be removed from the model. This means that equation (63d) is removed and $\boldsymbol{v}_{gy,p}$ is removed from (63c). Because the filter is a high pass filter the DC component of the signal is removed, thus the calibrated bias must also be removed from (63c). This new model is denoted $\boldsymbol{f}_{INS,f}(\boldsymbol{x}_k,\boldsymbol{v}_k,\boldsymbol{u}_k)$ and consists of equation (63a), (63b) and

$$\boldsymbol{q}_b^l[k{+}1]=\Big(\boldsymbol{I}+T\big(\bar{\boldsymbol{\Omega}}(\boldsymbol{E}_{gy}^{-1}(\tilde{\boldsymbol{\omega}}_{ib}^b[k]))+\bar{\boldsymbol{\Omega}}(\boldsymbol{v}_{gy,w}^b)\big)\Big)\boldsymbol{q}_b^l[k] \quad (69)$$

C. Positioning with Inertial and Aiding Sensors

To increase accuracy additional sensors will be used. The measurement equations for the magnetometer and barometer will be presented in this section. The measurement equations are given on the form

$$\boldsymbol{z}_k=\boldsymbol{h}_k(\boldsymbol{x}_k,\boldsymbol{w}_k) \quad (70)$$

1) Magnetometer as Aiding Sensor: The magnetometer measurement update approach is found in [29] and uses the fact that rotating the magnetic field vector in the body frame to the local-level frame with quaternions should be equal to the magnetic field vector obtained by the IGRF model. This yields

$$\begin{bmatrix}0\\ \mathbf{B}^l\end{bmatrix}=\boldsymbol{q}_b^l\otimes\begin{bmatrix}0\\ \mathbf{B}^b\end{bmatrix}\otimes\bar{\boldsymbol{q}}_b^l \quad (71)$$

where $\mathbf{B}^l$ is the magnetic field in the local-level frame, $\mathbf{B}^b$ is the magnetic field in the body frame and $\boldsymbol{q}_b^l$ is the quaternion that rotates from the body frame to the local-level frame. $\mathbf{B}^l$ is obtained from the IGRF model and $\mathbf{B}^b$ is measured by the magnetometer. The equation (71) has four dimensions, where the first dimension is zero on both sides of the equation. This equation is omitted in the final measurement update because it will only provide noise into the system. Multiplying the quaternion $\boldsymbol{q}_b^l$ on both sides of the equation (71) and replacing the quaternion product with the matrices found in (6) gives

$$\boldsymbol{0}=\big(\Omega(\mathbf{B}^l)-\bar{\Omega}(\mathbf{B}^b)\big)\,\boldsymbol{q}_b^l \quad (72)$$

We now define $\boldsymbol{v}_{IGRF}$ as a noise component that models the error between the IGRF model and the real world. The error model for the magnetometer is given in section IV-A4. Inserting the error model for the magnetometer and $\boldsymbol{v}_{IGRF}$ into the above equation yields

$$\begin{aligned}\boldsymbol{0}&=\big(\Omega(\mathbf{B}^l+\boldsymbol{v}_{IGRF})-\bar{\Omega}(\boldsymbol{E}_{ma}^{-1}(\tilde{\mathbf{B}}^b-\boldsymbol{b}_{ma,f})+\boldsymbol{v}_{ma})\big)\boldsymbol{q}_b^l\\ &=[0\;\boldsymbol{h}_{MAG}(\boldsymbol{x}_k,\boldsymbol{w}_k)]^T \quad (73)\end{aligned}$$

where $\boldsymbol{E}_{ma}=\boldsymbol{I}+\boldsymbol{S}_{ma}$ and $\boldsymbol{v}_{ma}$ is the scaled version of $\boldsymbol{n}_{ma}$. The covariance of $\boldsymbol{v}_{IGRF}$ is $\sigma_{IGRF}^2\boldsymbol{I}$ and the covariance for $\boldsymbol{v}_{ma}$ is $\boldsymbol{E}_{ma}^{-1}\boldsymbol{\Sigma}_{ma}\boldsymbol{E}_{ma}^{-T}$.

The magnetometer measurement update does not give full obeservability of the quaternion. The quaternion has three degrees of freedom, while the update only observes two of these. Rotations around the magnetic field vector are not sensed.

2) Altimeter as Aiding Sensor: To use the barometer as an aiding sensor we must expand the model by including a measurement update. Combining (43) and (57) and solving for $\tilde{p}$ yields

$$\tilde{p}=(1+S_{ba})P_0\left(1-h\frac{T_{grad}}{T_0}\right)^{\frac{g}{R\cdot T_{grad}}}+B_{ba}+v_{ba} \quad (74)$$

Equation (74) is denoted $h_{BAR}(\boldsymbol{x}_k,\boldsymbol{w}_k)$. The white noise n_{ba} has been renamed to v_{ba}.

The barometer measurement update makes the upwards position state observable. It will also make one degree of freedom of the velocity observable.

3) Magnetometer and Altimeter as Aiding Sensors: When using both aiding sensors the UKF select the update equation depending on which sensor data that are available. If only magnetometer data is available then we use (73), and (74) for

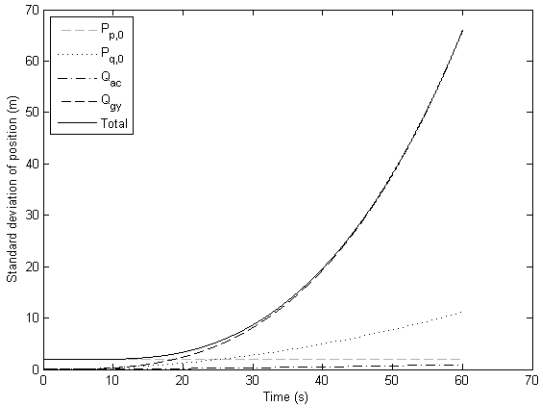

Fig. 2. The standard deviation of the position error caused by different noise sources. The model (5) has been simulated 100 times using the noise found in the sensor calibration.

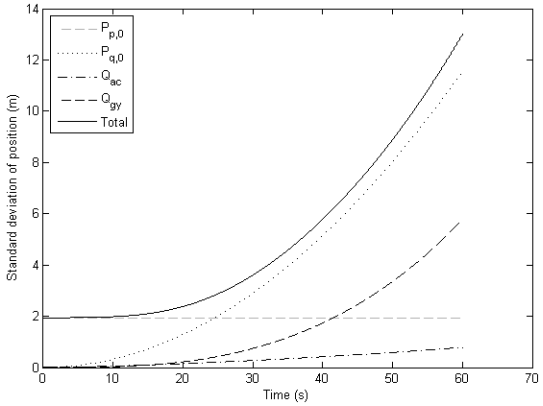

Fig. 3. The standard deviation of the position error caused by different noise sources. The model (5) has been simulated 100 times using the one tenth of the noise found in the sensor calibration.

barometer only. If both sensors has data available then we use the following update equation

$$\begin{bmatrix} \mathbf{0} \\ \tilde{p} \end{bmatrix} = \begin{bmatrix} \boldsymbol{h}_{MAG}(\boldsymbol{x}_k, \boldsymbol{w}_k) \\ h_{BAR}(\boldsymbol{x}_k, \boldsymbol{w}_k) \end{bmatrix} \tag{75}$$

Equation (75) is denoted $\boldsymbol{z}_k = \boldsymbol{h}_{BAR,MAG}(\boldsymbol{x}_k, \boldsymbol{w}_k)$. Combining the two measurements does not generally make more states observable.

V. Results

The results are divided into two parts, simulation results and a real world test.

A. Simulations

There has been two kinds of simulations. First we have simulated the model (5) to find how much each sensors contribute to the position error. Second we have conducted Monte Carlo simulations to find the position accuracy for different sensor configurations.

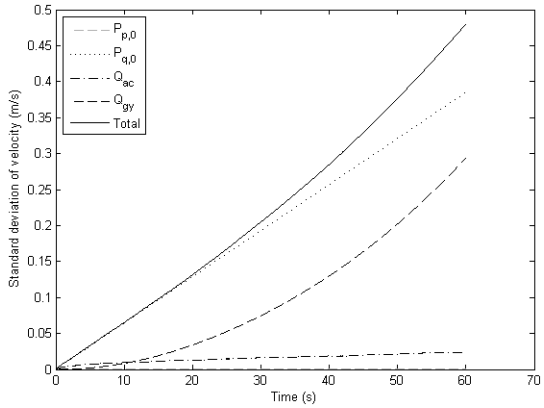

Fig. 4. The standard deviation of the velocity error caused by different noise sources. The model (5) has been simulated 100 times using the one tenth of the noise found in the sensor calibration.

1) Quantifying the Error Sources: We will now quantify the error sources in the inertial system without any aiding sensors. The process equation (5) is simulated Using Monte Carlo simulations. The individual noise sources are uncertainty in the initial position ($P_{p,0}$), noise errors from the sensors used in the QUEST algorithm ($P_{q,0}$), noise from the accelerometer (Q_{ac}) and noise from the gyroscope (Q_{gy}). Fig. 2 shows the standard deviation of the position error. The simulations are of a stationary system. The system has a standard deviation of the position error of approximately 65 m after 60 s. The main error source is the noise from the gyroscopes. The second largest error is the error from calculation of the initial attitude.

As the noise from the gyroscope is the main error source we want to find out how much the position error is reduced by using another sensor. Fig. 3 shows the same simulation as in Fig. 2, but the Angle Random Walk and Bias Instability coefficients has been reduced to one tenth. In this simulation the standard deviation for the position error has been reduced to 13 m after 60 s, and the error in calculation of the initial attitude is the main error source the first 60 s. Fig. 4 shows the standard deviation for the velocity with reduced noise from the gyroscopes. The error from the calculation of the initial attitude is the main error source, but it seems that the error from gyroscope noise increase faster and will eventually become the main error source.

2) Simulation of Filter Covariance: As seen in Part IV we want to test four different sensor configurations, respectively inertial sensors only, inertial sensors and barometer, inertial sensors and magnetometer and inertial sensors, barometer and magnetometer. In addition to the different sensors configurations we would like to test if filtering the gyroscope output might give an increased performance. Fig. 5 shows a Monte Carlo simulation of 8 runs for the standard deviation of the position error. High computational time prevented more runs. The position error is the difference between the position given by the UKF and the real position. The legend states which model and measurement updates that has been used. For instance in $f_{ins} + h_{bar}$ model (63) is used along with

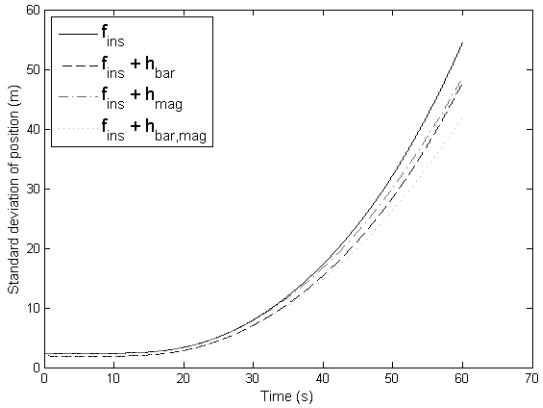

Fig. 5. The standard deviation of the position error for a selection of different sensor configurations. This is the result of 8 Monte Carlo runs.

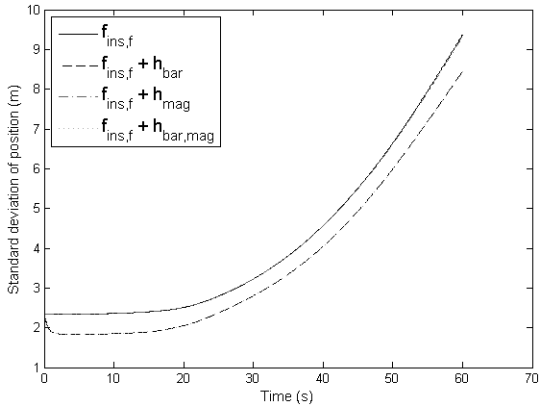

Fig. 6. The standard deviation of the position error for a selection of different sensor configurations. This is the result of 8 Monte Carlo runs.

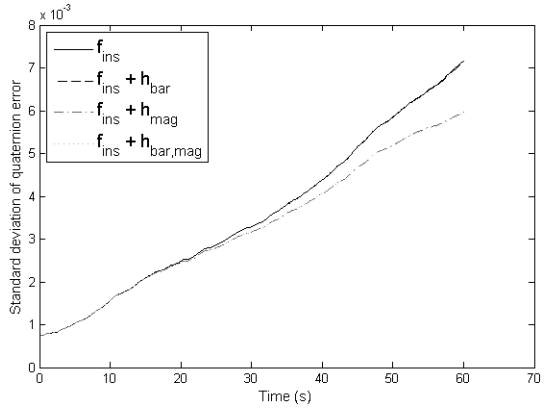

Fig. 7. The standard deviation of the quaternion error for a selection of different sensor configurations. This is the result of 8 Monte Carlo runs.

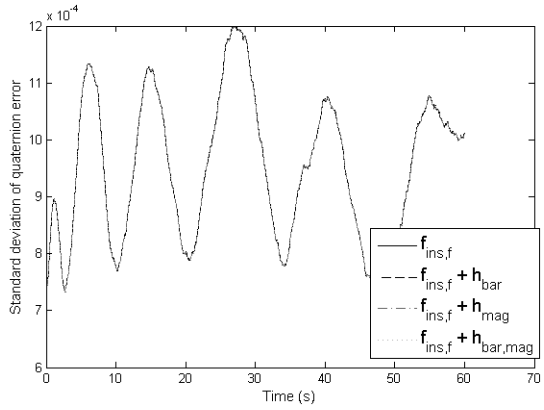

Fig. 8. The standard deviation of the quaternion error for a selection of different sensor configurations. This is the result of 8 Monte Carlo runs.

the measurement update (74). The standard deviation when only using inertial sensors are close to the results found in Section V-A1, where we only simulated the navigation equations and not the UKF. Additional sensor decrease the standard deviation. When using barometer as aid sensor the standard deviation is decreased to just bellow 50 m after 60 s. When using magnetometers the standard deviation is a little bit higher than when using a barometer, but it is increasing slower and will eventually become lower that using a barometer. The error is lowest when using both barometer and magnetometers giving a standard deviation of approximately 42 m after 60 s.

Fig. 6 shows the same as Fig. 5 except that the gyroscope output has been filtered. This gives a large increase in the system accuracy. When the system is moving the error might become larger, because important information from the gyroscopes might have been filtered out. The standard deviation of the position error is below 9.5 m after 60 s when only using inertial sensors. When adding a barometer this value drops to 8.5 m. Magnetometers have little impact on position accuracy, most likely because the noise from the magnetometers are higher than the noise from the filtered gyroscopes.

Fig. 7 and Fig. 8 shows the standard deviation of the quaternion error from the same Monte Carlo simulation as Fig. 5. The linear incresing error in Fig. 7 might be a bias error because the gyroscope bias is not stable. In Fig. 8 the bias is filtered away. The magnetometer decreases the error in 7, but not in Fig. 8

B. Preliminary Real World Test

Figure 9 and 10 shows the total position error from preliminary tests. The total position error is in this case the length of the vector that starts in the initial position and ends in the calculated position. Using inertial sensors with filtered gyroscope output and barometer measurement updates yields the best result with an error of approximately 58 m after 60 s. All the results are much larger than found in the simulations. The gyroscope bias varies with time and we use a constant bias compensation, which may lead to some errors. Even though the magnetometers has been calibrated on the rate board there still might be some magnetic disturbance that creates a error in the initial attitude. These results are preliminary and the reason for the large errors are therefor not yet identified.

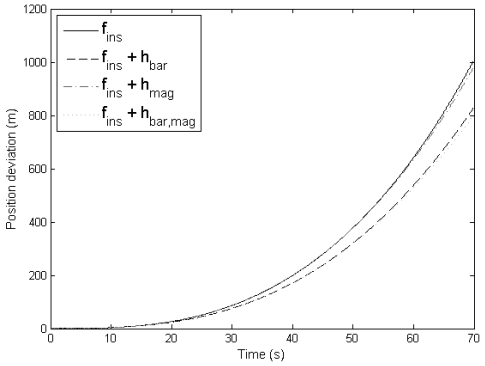

Fig. 9. Calculated deviation from initial position using real world data

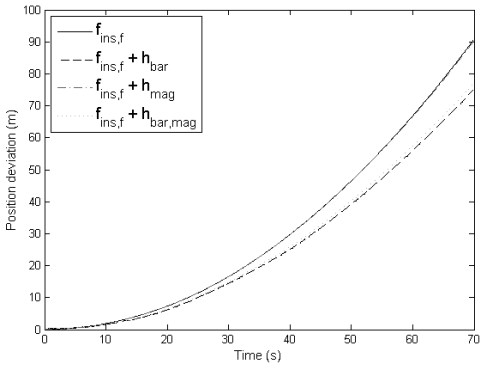

Fig. 10. Calculated deviation from initial position using real world data

VI. Conclusions

Simulations has shown that the standard deviation of the position error for a stationary unit is 65 m after 60 s. If the gyroscope was replaced with a gyroscope with only one tenth of the noise, the error can be reduced to 13 m. Other simulations show that the standard deviation of the position error could be reduced to 8.5 m if gyroscope output is filtered. This is a significant improvement, but it is unknown if the results will be this good for a moving platform. When using unfiltered gyroscope output the best performance is obtained by using magnetometers and barometer as aid sensors. Using the aiding sensors decreased the standard deviation of the position with approximately 13 m or 23 %. This indicates that there is much to gain by using aiding sensors.

The stationary real world test drift away from the initial position much faster than the simulations. The real world test are only preliminary tests, therefor we are unable to draw any conclusions from them.

For indoor navigation a uncertainty of 10 m might be needed to distinguish between different rooms. For other applications a higher uncertainty might be suffice. If we define the needed accuracy to be 10 m, simulation has shown that the system can have this accuracy for 60 seconds. If longer times are needed other sensors must be found. The gyroscopes is the main error source, therefore these sensors should be replaced if better accuracy is needed. For the unit to work with real data, the problems mentioned in Section V-B needs to be addressed.

References

[1] D. Goehl and D. Sachs, "Motion sensors gaining inertia with popular consumer electronics," InvenSense, Inc., Tech. Rep., http://invensense.com/mems/glossary.html.

[2] P. Sherman and S. Holmes, "Personal navigation system," in *Technical report NATRICK/TR-06/004, Draper Laboratory*, 2005.

[3] Q. Ladetto, V. Gabaglio, and B. Merminod, "Two different approaches for augmented gps pedestrian navigation," in *International Symposium on Location Based Services for Cellular Users, Locellus 2001*, 2001.

[4] ——, "Combining gyroscopes, magnetic compass and gps for pedestrian navigation," in *International Symposium on Kinematic Systems in Geody, Geomatics and Navigation (KIS 2001) , Banff, Canada, June 5-8, pp. 205-212.*, 2001.

[5] S. Godha and G. L. M. E. Cannon, "Integrated gps/ins system for pedestrian navigation in a signal degraded environment," in *ION GNSS 2006, Forth Worth TX, 26-29 September 2006*, 2004.

[6] S. Beauregard, "Omnidirectional pedestrian navigation for first responders," in *WPNC'07, pages 33?36, 2007*, 2007.

[7] Q. Ladetto, J. van Seeters, S. Sokolowski, Z. Sagen, and B. Merminod, "Digital magnetic compass and gyroscopes for dismounted soldier positioning & navigation," in *NATO-RTO meetings, Istanbul, Turkey, 2002*. NATO, 2002.

[8] E. Bekir, *Introduction to Modern Navigation Systems*. World Scientific Publishing, 2007.

[9] B. Hofmann-Wellenhof, K. Legat, and M. Weiser, *Navigation: Principles of positioning and guidance*. Springer-Verlag Wien New York, 2003.

[10] J. A. Farrell and M. Barth, *The Global Positioning System & Inertial Navigation*. The McGraw-Hill Companies, Inc., 1999.

[11] O. Egeland and J. T. Gravdahl, *Modeling and Simulation for Automatic Control*. Tapir trykkeri, 2002.

[12] K. Mathiassen, "Positioning with inertial sensors and aid sensors when loosing gps fix," Master's thesis, Norwegian University of Science and Technology, 2010.

[13] M. D. Shuster and S. D. Oh, "Three-axis attitude determination from vector observations," in *Journal of Guidance and Control Volume 4 Number 1*, 1981.

[14] S. M. ans Stefan Maus, "International geomagnetic reference field - the tenth generation," in *Earth Planet Space issue 57 page 1135-1140*, 2005.

[15] E. E. Wan and R. van der Merwe, "The uncented kalman filter for non-linear estimation," in *IEEE 2000 Adaptive Systems for Signal Processing, Communications, and Control Symposium*. IEEE, 2000.

[16] S. J. Julier, "The scaled uncented transformation," in *Proceedings of the American Control Conference*. IEEE, 2002.

[17] E. Kraft, "A quaternion-based unscented kalman filter for orientation tracking," in *Proceedings of the Sixth International Conference of Information Fusion*, vol. 1, 2003, pp. 47–54.

[18] Intersema, *Using MS5534 for altimeters and barometers*.

[19] (2010, March). [Online]. Available: http://www.ngdc.noaa.gov/IAGA/vmod/igrf.html

[20] (2010, March) Universidade do Algarve. [Online]. Available: http://w3.ualg.pt/~jluis/mirone/

[21] F. Lowes. The international geomagnetic reference field: A 'health' warning. [Online]. Available: http://www.ngdc.noaa.gov/IAGA/vmod/igrfhw.html

[22] K. Mathiassen, "System for posisjonering ved bruk av treghetsnavigasjon," 2009, project Report.

[23] Fastrax, "UP500 datasheet," 2008.

[24] A. Devices, "ADIS16400/ADIS16405 datasheet," 2009.

[25] Intersema, "MS5534C Barometer module datasheet," 2008.

[26] R. B. Langley, "Dilution of precision," *GPS World*, pp. 52–59, May 1999.

[27] D. H. Titterton and J. L. Weston, *Strapdown Inertial Systems Technology*. The American Institute of Aeronautics and Astronautics and The Institution of Electrical Engineers, 2004.

[28] *IEEE Standard Specification Format Guide and Test Procedure for Single-Axis Interferometric Fiber Optic Gyros*. The Institute of Electrical and Electronics Engineers, Inc., 1998.

[29] Y. Luo, C. C. Tsang, G. Zhang, Z. Dong, G. Shi, S. Y. Kwok, W. J. Li, P. H. W. Leong, and M. Y. Wong, "An attitude compensation technique for a mems motion sensor based digital wristing intrument," in *IEEE International Conference on Nano/Micro Engineered and Molecular Systems*. NASA Goddard Space Flight Center, Greenbelt, MD, 2006.